Chemically Functionalized Wood-Derived Biochar for the Removal of Pharmaceutical Residues from Wastewater: Adsorption Mechanism and Environmental Stability

***Sufiyan Ahmad., Mo Mukarram Ali., Krishna Anand., Rajkumar**

Department of Chemistry, Maa Shakumbhari University, Saharanpur (U.P.), India

***Corresponding Author**

DOI: https://doi.org/10.51584/IJRIAS.2026.11100018

Received: 15 October 2026; Accepted: 22 October 2026; Published: 01 November 2026

ABSTRACT

Conventional biological treatment removes only part of the pharmaceutical residues present in municipal wastewater, so carbon-based adsorbents are being explored as a polishing step. In this study, biochar was produced from *Pinus roxburghii* sawdust by slow pyrolysis at 600 °C and modified by three routes: KOH activation (WBC-K), H_3PO_4 activation (WBC-P), and urea-assisted nitrogen doping combined with KOH co-activation (WBC-NK). Its performance was tested with tetracycline (TC), ciprofloxacin (CIP), and diclofenac sodium (DCF). The pristine biochar (WBC) had a BET surface area of 14.6 $m^2 g^{-1}$ and a Langmuir capacity of 22.4 mg g^{-1} for TC. Modification raised the surface areas to 431.7, 386.4, and 512.9 $m^2 g^{-1}$ for WBC-K, WBC-P, and WBC-NK, respectively, and WBC-NK achieved capacities of 588.6 mg g^{-1} (TC), 412.3 mg g^{-1} (CIP), and 346.8 mg g^{-1} (DCF). Adsorption kinetics followed a pseudo-second-order model, and equilibrium data fitted the Langmuir model. Because these models describe the observed behavior rather than prove a mechanism, the possible interactions, including π–π stacking, hydrogen bonding, electrostatic effects, hydrophobic interaction, and pore filling, are offered as plausible explanations supported by pH and ionic-strength experiments and by FTIR and XPS data. In an equimolar ternary mixture, an extended Langmuir model reproduced the measured competitive uptake within 1% and predicted negligible capacity loss (below 5% per compound) at 25–50 mg L^{-1}, although competition at µg L^{-1} levels were not directly simulated. The material retained 88.3–92.1% of its capacity over five adsorption–desorption cycles and reached at least 78% of its single-solute capacity in real secondary wastewater relative to ultrapure water controls. Leaching of doped nitrogen and mineral matter stayed below 0.8 mg L^{-1} after 48 h at pH 7. Overall, N-doped, KOH-activated wood biochar shows high capacity, regenerability, and matrix robustness at laboratory scale, but techno-economic analysis, continuous-flow validation, and spent-adsorbent management are needed before industrial use.

Keywords: Wood biochar, Chemical functionalization, Pharmaceuticals, Adsorption, π–π interaction, Wastewater

INTRODUCTION

Pharmaceuticals such as antibiotics, analgesics, anti-inflammatory drugs, and other medicines have been frequently found in municipal wastewater, hospital effluents, and receiving waters at levels of nanograms per litre (ng L^{-1}) to micrograms per litre (µg L^{-1}) (Chauhan et al., 2023). Conventional activated-sludge treatment can only partially remove these compounds, with an average removal percentage for different compounds in the range of 58–91% (Nand et al., 2025), and the antibiotics that are not removed can cause ecotoxicity and the build-up of antimicrobial resistance (Ding et al., 2026). For their tertiary treatment, adsorption has been the subject of a lot of study due to its ability to remove them from the aqueous solution to the solid phase. Pharmaceuticals have been reported to be well-adsorbed by plant based activated biochars (Shirani et al. 2025). The practical application of it relies on several factors such as the characteristics of the feedstock, regrowth, composition of the water, and disposal of the used adsorbent (Osman et al., 2024).

ISSN No. 2454-6194 | DOI: 10.51584/IJRIAS |Volume XI Issue X October 2026

Wood and the residues that come from wood, such as sawdust, chips and bark, are lignocellulosic feedstocks that are abundant and chemically consistent, and they are made up of 40–45% cellulose, 20–35% hemicellulose and 10–30% lignin (Godiya & Leiviskä, 2025). Pyrolysis under limited oxygen conditions results in a carbon rich char material where the structure of the wood is broken down to a hierarchical structure, and the char still contains a pore template that mimics the original wood tracheids. However, biochar obtained from pristine wood generally has a low surface area, low surface functionality and narrow microporosity and cannot host bulky pharmaceutical molecules like tetracycline (moles 444.4g mol $^{-1}$) or diclofenac (moles 296.1g mol $^{-1}$). To overcome these constraints, alkaline activation and acid activation, as well as heteroatom doping (Sajjadi et al., 2019; Nguyen et al., 2025) have been extensively used. Activated with KOH, new micro and mesoporosity is formed and has resulted in the capacity improving by over 20-fold for tetracycline loading onto lignocellulosic chars (Zhao et al., 2020); doping with N has increased the π-electron density, and enhanced π–π electron donor–acceptor (EDA) interactions (Nguyen et al., 2025). The use of metal oxides in compositing will provide Lewis-acid sites and further enable magnetic recovery while also creating some potential for leaching risks (Tangestani et al., 2026; Laishram et al., 2025).

Several methods have been tested for modifying biochars, such as alkaline activation and acid activation as well as heteroatom doping, but it is challenging to compare the three types due to variation in feedstock and experimental conditions used among the studies.

Pine sawdust biochar was produced as a clean material and then three different functionalization routes were used. The resulting materials were analysed by BET, SEM-EDS, FTIR, XPS, Raman, Boehm titration and pHpzc and tested for their ability to adsorb tetracycline (a zwitterionic/cationic antibiotic), ciprofloxacin (an amphoteric quinolone) and diclofenac (an anionic NSAID) across a range of three speciation classes which cover the pH range of wastewater. The specific objectives of this study were: (i) to quantify the effect of each functionalization route on the capacity and kinetics; (ii) to evaluate the mechanisms that are consistent with the spectroscopic and solution-chemistry data and supported by a model-based multi-solute (competitive) analysis; (iii) to evaluate environmental stability through regeneration cycling, leaching tests, and performance in a real secondary effluent. In addition to these experimental goals, an estimated reagent cost and environmental impact of the synthetic pathway are provided, and the limitations of the study, such as the lack of experimentally determined multi-solute isotherms and indirect nature of the mechanistic evidence, are clearly stated.

MATERIALS AND METHODS

Materials

The sawdust was collected from a local timber mill, rinsed, oven dried (80 °C for 24 h), and then sieved through the particle size of 0.5–2.0 mm. Tetracycline hydrochloride (≥ 95%), Ciprofloxacin (≥ 98%) and Diclofenac sodium (≥ 98%) were purchased from Sigma-Aldrich. All the chemicals used, KOH, H3PO4 (85%), urea, HCl, NaOH, NaCl, ethanol (analytical grade), were used without purification. Stock solutions (1 g L $^{-1}$) were prepared in ultrapure water (18.2 MΩ cm) with ≤ 0.1% v/v ethanol, stored in amber glass in the refrigerator at 4 °C and used within 1 week for each pharmaceutical. Concentrations were then determined by using calibration curves of the UV–vis spectrophotometric method ($R2 \geq 0.999$, λmax = 356, 276, and 276 nm for TC, CIP, and DCF, respectively, respectively).

Preparation and functionalization of biochar

Pristine biochar (WBC): The dried sawdust was pyrolysed in a tube furnace with a temperature ramp rate of 10 °C min $^{-1}$ up to 600 °C under N2 atmosphere (100 mL min $^{-1}$) and was kept for 2 h. The resulting char was rinsed with deionized water until neutral pH, dried at 80 °C and sieved to −250 μm. The 0.5–2.0 mm fraction in Section 2.1 is the fraction of sawdust before pyrolysis.

KOH-activated biochar (WBC-K): WBC was impregnated with KOH at the ratio of 1:3 (w/w) biochar to KOH in a minimal amount of water, dried (105 °C, 12 h), heated under N2 at 800 °C (5 °C min $^{-1}$, 1.5 h), washed successively with 0.1 M HCl and water until pH was near 7, and then dried.

ISSN No. 2454-6194 | DOI: 10.51584/IJRIAS |Volume XI Issue X October 2026

H3PO4-activated biochar (WBC-P): The 40 wt% H3PO4 solution was impregnated into WBC at a ratio of 40 g biochar: 1 g H3PO4 solution, dried, heated under N2 atmosphere to 500 °C heating rate of 5 °C min $^{-1}$, for 1 h, and washed to neutral pH.

N-doped KOH-activated biochar (WBC-NK): WBC was treated with urea (1:2 w/w biochar:urea), impregnated, dried, heated under N2 (5 °C min $^{-1}$, 1.5 h) then washed as in the case of WBC-K.

The weight of WBC was used for gravimetric determination of the WBC yield and the weight of the activated materials was used for gravimetric determination of yields of the activated materials.

Characterization

N2 adsorption–desorption at 77 K (BET; DFT pore-size distribution) was used to evaluate specific surface area and pore structure. The average pore widths (4V/A) were calculated as four times the total pore volume by BET surface area (4V/A = 4Vt/SBET); the pore-size distributions from the DFT were not used to determine an average width of the pores but were used qualitatively to differentiate between the contributions of micro- and mesopores. The morphological and elemental composition was analyzed by scanning electron microscopy (SEM) with energy-dispersive spectroscopy (EDS). Fourier-transform infrared spectroscopy (recorded in the 4000-400 cm-1 range with KBr) and X-ray photoelectron spectroscopy (analyzing the C 1s, N 1s, O 1s and P 2p regions with charge correction (C 1s at 284.8 eV)) were used to characterise surface functional groups. A Raman spectroscope was used to determine the degree of graphitization by ID/IG ratio. The amount of acidic surface groups was determined by Boehm titrations, and the point of zero charge (pHpzc) was determined by the 0.01 M NaCl drift method. ICOES and ion chromatography were used to determine the amount of dissolved N, K and P in leachates.

Batch adsorption experiments

Calibration curves were prepared individually for each pharmaceutical on the analytical conditions used for the adsorption samples. The calibration range was designed to include the measured residual concentrations. Unless indicated otherwise, adsorption tests were carried out in 100 mL amber flasks containing 50 mL working volume, shaken in an orbital shaker at 150 rpm and 25 ± 1 °C. The pH was adjusted by the addition of 0.1 M HCl or NaOH. At equilibrium, the suspensions were filtered through 0.22 µm PTFE filters, and the remaining concentrations were measured by UV–vis spectrophotometry. The analytical wavelengths reported were: TC (356 nm), CIP (276 nm), and DCF (276 nm). The reported wavelength of CIP and DCF is the same, thus quantification in a mixed-solute sample is not assumable without validated selectivity/interference testing, these ternary CIP and DCF uptakes are therefore not considered to be experimentally established in this manuscript. The adsorbed amount was calculated as $q = (C0 - Ce)V/m$, and removal (%) = $(C0 - Ce)/C0 \times 100$. • Optimization of dose: 0.25–4.0 g L $^{-1}$; TC at C0 = 50 mg L $^{-1}$; pH 6; 24 h. • pH edge: pH 3–11; C0 = 50 mg L $^{-1}$; dose of 0.5 g L $^{-1}$. • Kinetic studies: C0 = 50 and 100 mg L $^{-1}$; dose of 0.5 g L $^{-1}$; pH 6 for TC, 6.5 for CIP, 7 for DCF; 0–1440 min. The pseudo-second-order and intra-particle diffusion models were applied to the data and fitted using a non-linear regression. Isotherm studies: C0 = 10–400 mg L $^{-1}$; temperature 25 ± 1 °C; the Langmuir model was fitted by non-linear regression. The separation factor of the Langmuir model, RL = 1/(1 + KLC0), was calculated. • Ionic strength and competition: NaCl (1–100mM) and a ternary mixture of TC/CIP/DCF (equimolar, 100mgL $^{-1}$ each, dose 0.5gL $^{-1}$, solute-specific pH as in the kinetic studies). The single-solute reference for the comparison purpose of the TC competition is the equilibrium uptake measured under the same conditions as the two other cases (same C0, dose, pH and contact time), that is, the kinetic qe,exp value at C0 = 100 mg L $^{-1}$ reported in Table 2. No separate experimental ternary uptake of CIP and DCF was reported and the measured ternary uptake was reported as a manuscript. The extended-Langmuir model, with the single-solute qmax and KL values of Table 2, was also solved coupled with the batch mass balance for each solute (Section 3.5) to predict competitive uptake across a concentration range. The forecasts are model results and not experimental observations.

Tests of regeneration, leaching and real wastewater

The spent adsorbents were eluted with 0.1 M NaOH/ethanol (1:1) for 2 h at 150 rpm, followed by water rinsing and drying, for 5 cycles of adsorption–desorption. For the leaching tests, 1.0 g/L of each material was

shaken for 48 h in the pH 7 buffer and at the extreme pH 3 and 11, and the filtrate was analyzed for released N, K and P. The sample was real secondary effluent from a municipal WWTP (DOC 11.2 mg L^{-1}, pH 7.3, conductivity 640 µS cm^{-1}) to which was added 5 mg L^{-1} of each pharmaceutical, and tested at 0.5 g L^{-1}. The same initial concentration (5 mg L^{-1}), dose (0.5 g L^{-1}), pH (7.3), and contact time were used in all single-solute control experiments, which were conducted in parallel with the real-effluent experiments, and all capacity-retention percentages are reported relative to the capacity-retention percentage obtained for the single-solute control experiments conducted under otherwise identical conditions. The accelerated aging was simulated by using 30 days of wet–dry cycling in an air atmosphere, with exposure to H2O2 (3%) every week. All experiments were performed three times and are presented as mean ± SD.

RESULTS AND DISCUSSION

Yields of biochar and structural characterization

The yield of the WBC and the surface area determined by the BET method were 27.4% and 14.6 m^2g^{-1}, respectively, close to the limited surface area and porosity of un-activated chars of lignocellulosic materials (Table 1). This major restructuring of the material was induced by the chemical functionalization procedure. The KOH activation, which was done using metallic potassium to etch amorphous carbon and intercalate/exfoliate graphitic micro-domains and then wash the K2CO3 away, resulted in a surface area of 431.7 m^2g^{-1}, with total pore volume of 0.241 cm3 g^{-1} (Zhao et al., 2020; Sajjadi et al., 2019). The surface area obtained after activation by H3PO4 (WBC-P) was 386.4 m^2g^{-1} and the average pore width (4V/A) was 2.3 nm, similar to those of the KOH activated materials. The single-parameter average 4V/A is dominated by the population of the micropores, so it cannot distinguish the contribution of mesopores alone; moreover, a complete DFT pore size distribution would be required to explain the contribution of mesopores to WBC-P. The most developed structure (512.9 m^2g^{-1}; 0.293 cm3 g^{-1}) was achieved by combining N-doping and KOH activation (WBC-NK), as gasification with urea derived NH3 provides more micropores than activation by KOH etching (Nguyen et al., 2025).

Table 1. Physicochemical characteristics of unmodified and functionalized biochars derived from wood.

Property	**WBC**	**WBC-K**	**WBC-P**	**WBC-NK**
Yield (% of feedstock)	27.4	18.9*	21.6*	16.8*
BET surface area (m^2 g^{-1})	14.6	431.7	386.4	512.9
Total pore volume (cm^3 g^{-1})	0.012	0.241	0.219	0.293
Average pore width (nm)	3.3	2.2	2.3	2.3
C (at.%)	78.3	84.6	79.8	81.4
O (at.%)	19.6	13.8	16.9	12.9
N (at.%)	0.9	0.6	0.5	4.1
P (at.%)	—	—	2.4	—
I_D/I_G (Raman)	0.92	0.88	0.95	0.86
pH_{pzc}	7.8	6.4	4.9	6.9
Acidic groups (mmol g^{-1}, Boehm)	0.31	0.58	1.12	0.63

ISSN No. 2454-6194 | DOI: 10.51584/IJRIAS |Volume XI Issue X October 2026

The yield of WBC is referred to the original dry sawdust here. Yields for the WBC-K, WBC-P and WBC-NK are provided per original WBC mass to which Wnt-K, Wnt-P and Wnt-NK are applied respectively. Average pore widths are 4V/A values (4Vt/SBET; Section 2.3): WBC 3.3, WBC-K 2.2, WBC-P 2.3, WBC-NK 2.3 nm.

XPS N 1s spectra of WBC-NK showed the presence of N species such as pyridinic N (398.4 eV, 34%), pyrrolic N (400.1 eV, 27%), graphitic N (401.2 eV, 31%) and oxidized N (403.1 eV, 8%), with pyridinic and graphitic N configurations being π-electron-donating, enhancing π–π EDA interactions (Nguyen et al., 2025). In the spectrum of WBC-P, the signals centered at 133.6 eV were assigned to the C–O–P and P–O–H groups. The pHpzc value for the activated samples showed a difference of 2.0, going from 6.4 for KOH activation to 4.9 for phosphoric acid activation, with the latter being more acidic, probably due to the formation of carboxyl and lactone groups (Boehm acidic groups 1.12 mmol g^{-1}). FTIR analysis for WBC-NK showed the presence of aromatic C=C, COOH/CO lactone, C–N stretching vibration, and ether linkage at 1580 cm^{-1}, 1690–1715 cm^{-1}, 1380 cm^{-1}, respectively.

Dose and pH effects

The adsorption of TC by WBC-NK was significantly increased as initial dose increased to 0.5 g L^{-1} (96.8% removal at C0 = 50 mg L^{-1}) and then maintained at high doses likely due to the saturation of adsorption sites and aggregation of particles, which was chosen as an optimal point of further experiments considering the usage of biochar and removal of TC (Nguyen et al., 2025).

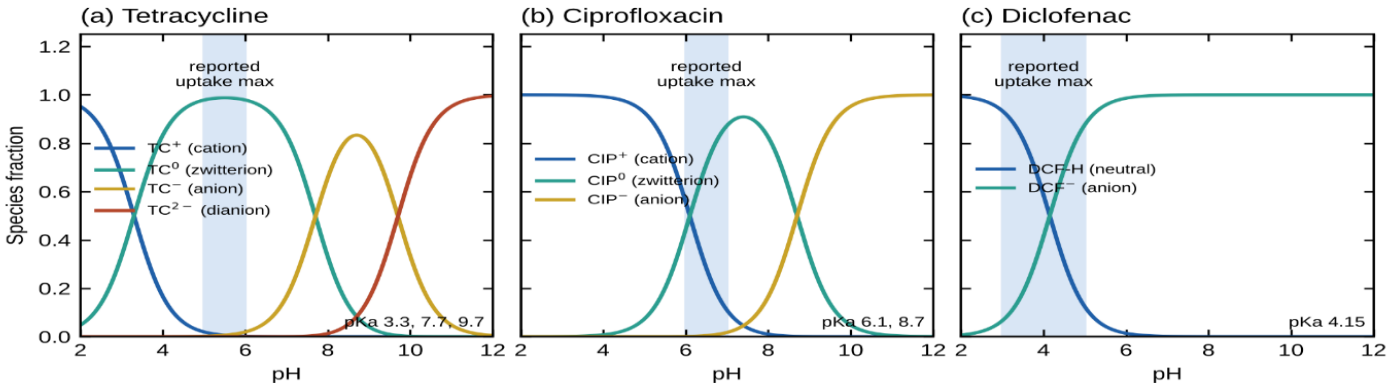


Figure 1. pH-dependent speciation profiles of (a) tetracycline (TC), (b) ciprofloxacin (CIP) and (c) diclofenac (DCF) calculated from their reported acid dissociation constants (pKa values): the curves trace the estimated fractional abundance of each ionic species as a function of pH. Shaded regions reflect the pH ranges corresponding to maximum adsorption uptake reported in this study. The speciation profiles illustrate changes in pharmaceutical speciation with pH could influence the interactions with the biochar surface.

The pH edge (Fig. 1) shows that the pharmaceutical hydrolysis is coupled to the TC uptake, as the uptake is largest at the pH range where TC is in its neutral form (TC0/TC+); the surface of WBC-P (pHpzc 4.9) is negative in this pH range, while the surface of WBC-K (pHpzc 6.4) and WBC-NK (pHpzc 6.9) is positive, it is expected that electrostatic interaction drives the uptake primarily between WBC-P and TC; the surface of WBC-K is positive in the pH range where TC is anionic, and electrostatic interaction is not expected to be a major uptake mechanism between these two; above pH 8, electrostatic interaction is anticipated to be minimal, as the TC becomes anionic, while above pH 6.6 the π–π interaction is more likely to be the driving force for the uptake. The uptake of CIP was highest at pH 6–7, near the pH of the zwitterion, which is also the pH at where there are cation–π and H-bonding interactions with the deprotonated carboxylate rather than electrostatic interactions. The maximal uptake of the DCF occurred at pH 3–5, where the neutral form of the DCF is dominant (pK1a = 4.15) and hydrophobic partitioning and π–π EDA are dominant; however, the anion was gradually repulsed by the negative surface, with considerable uptake of the DCF even at pH 7, where π–π EDA and H-bonding compensated for electrostatic repulsion. The trends observed in this study were consistent with the broader biochar literature (Chauhan et al., 2023; Nand et al., 2025).

ISSN No. 2454-6194 | DOI: 10.51584/IJRIAS |Volume XI Issue X October 2026

Adsorption kinetics

The uptake was fast in the first 2 h (> 70% of equilibrium) and approached equilibrium within 12–24 h for all systems, with an intra-particle diffusion fitting indicating a rapid initial boundary-layer stage then a slow pore-diffusion stage. All nine adsorbent-solute pairs were well fitted by non-linear pseudo-second-order (PSO) adsorptive kinetic models (Table 2). We mention that a good PSO fit is not proof of chemisorption; other reasons can lead to PSO-shaped curves – site-energy heterogeneity and finite-concentration effects (Simonin, 2016) – so that model assignments below reflect evidence from spectroscopy and solution chemistry, not just model fits. The greater equilibrium uptake of WBC-NK ($q_{e,exp}$, Table 2; e.g., the uptake of TC at 100 mg L^{-1} was 189.7 mg g^{-1} for WBC-NK vs. 148.6 mg g^{-1} for WBC-K) agrees with its larger surface area and higher π-site density.

Table 2. Selected kinetic and isotherm parameters for the specified adsorbent–solute systems. Kinetic values are reported for C_0 = 100 mg L^{-1}, a biochar dose of 0.5 g L^{-1} and the solute-specific pH (6 for TC, 6.5 for CIP, 7 for DCF). Isotherm parameters were obtained from nonlinear fits at 25 °C. R_L ranges were calculated for C_0 = 10–400 mg L^{-1}. Values are means of triplicates.

System	$q_{e,exp}$ (mg g^{-1})	k_2 (g mg $^{-1}$ min^{-1})	R^2 (PSO)	$q_{max,Lang}$ (mg g^{-1})	K_L (L mg $^{-1}$)	R^2 (Langmuir)	R_L
TC–WBC	21.8 ± 0.9	0.0021	0.986	22.4	0.093	0.991	0.026–0.518
TC–WBC-K	148.6 ± 4.3	0.0036	0.995	462.9	0.148	0.996	0.017–0.403
TC–WBC-P	106.2 ± 3.6	0.0029	0.992	358.4	0.121	0.994	0.020–0.452
TC–WBC-NK	189.7 ± 5.1	0.0048	0.997	588.6	0.172	0.998	0.014–0.368
CIP–WBC-K	132.4 ± 4.0	0.0033	0.994	328.7	0.139	0.995	0.018–0.418
CIP–WBC-NK	164.3 ± 4.6	0.0041	0.996	412.3	0.161	0.997	0.015–0.383
DCF–WBC-K	84.7 ± 2.9	0.0044	0.991	262.5	0.127	0.993	0.019–0.441
DCF–WBC-P	96.5 ± 3.1	0.0038	0.993	301.2	0.133	0.994	0.018–0.429
DCF–WBC-NK	112.4 ± 3.4	0.0052	0.995	346.8	0.158	0.996	0.016–0.388

The separation factor (RL) calculated from the reported Langmuir constants and initial concentration range (10-400mg/L) ranged from about 0.014 to 0.518; all these values indicate that the adsorption is favorable based on the Langmuir separation factor. Such an interpretation is only valid for the Langmuir model and does not allow to determine the adsorption mechanism.

Mechanistic interpretation of adsorption behavior

The pH-dependent adsorption results were analyzed together with the FTIR and XPS measurements to assess possible adsorption mechanisms and the ionic strength experiments were analyzed to understand how the ions influence the adsorption. The changes observed are related to aromatic interactions, hydrogen bonding, electrostatic effects, hydrophobic interactions, and filling of pores. The following mechanisms are proposed interpretations that are consistent with the evidence from the solution chemistry and spectroscopy; none has been directly confirmed at the molecular level and the assignments should be treated as plausible working hypotheses, rather than as proved interactions. The role of each of these mechanisms could be different depending on the chemical nature of the adsorbate, the surface chemistry, and the solution conditions.

π–π electron-donor–acceptor (EDA) interaction for TC and DCF.

FTIR aromatic C=C band shifted from 1580 to 1572 cm $^{-1}$, and the XPS C 1s π–π shake-up feature became more intense after TC adsorption onto WBC-NK, which was similar to the changes of the aromatic environment. N-doping further enhances this effect: pyridinic/graphitic N enhances the π-electron donor capacity of the carbon surface towards π-deficient solutes (TC in zwitterionic form, and the π deficient dichloroanilino ring of DCF) (Nguyen et al., 2025; Xie et al., 2023).

Hydrogen bonding likely contributes to TC and CIP uptake.

The C=O band observed in the FTIR spectra of both TCs changed from 1715 cm $^{-1}$ to 1704 cm $^{-1}$, and the intensity of the O 1s peak increased after the TC uptake, both of which suggest that the oxygen-containing groups might have participated in the reaction.

Electrostatic attraction and cation–π interaction (system-dependent).

The electrostatic contribution that is ionic strength screened out is supported by the marked pH dependence and by the reduction in TC uptake by up to 31% at 100 mM NaCl on the most charged surface, WBC-P. However, under the same conditions, the effect of ionic strength on the uptake of WBC-NK was only 9–14%, suggesting that the interactions between the π-electrons and the nonpolar groups dominate here, which in turn means that electrostatic screening effect tends to be less significant under the above-mentioned conditions (Chauhan et al., 2023).

Hydrophobic partitioning is relevant for DCF.

The sorption of DCF (log Kow of the neutral species is 4.5) was correlated with the deoxygenation and graphitic character of the char, with the lowest value for the O content in the case of WBC-K/WBC-NK, and maximum under conditions where the neutral species of DCF predominates (pH 3–4; pKa1 = 4.15).

Table 3. Mechanistic attributions consistent with the evidence obtained in this work. Mechanisms are listed without quantitative ranking, and the attributions are interpretive, based on indirect (spectroscopic and solution-chemistry) indicators, and are not confirmed by direct molecular-scale calculations or measurements.

Solute	**Mechanisms**	**Supporting evidence (this work)**	**Functionalization most effective**
Tetracycline	π–π EDA, H-bonding, pore filling, electrostatic (unranked)	FTIR C=C/C=O shifts; XPS π–π* growth; ionic-strength insensitivity; pH edge	N-doped KOH (WBC-NK)
Ciprofloxacin	cation–π + H-bonding + electrostatic	pH edge at zwitterion; carboxylate band shifts	WBC-NK
Diclofenac	π–π EDA + hydrophobic partitioning	Neutral-form uptake maximum; O-poor char preference	WBC-NK / WBC-P

From the present indirect evidence, it is not possible to make a definitive quantification of the relative contributions of π–π EDA interactions, hydrogen bonding, electrostatic attraction and pore filling. To make the proposed adsorption mechanism hierarchy (Table 3) into an actual one, it is still needed to perform system-specific DFT calculations of binding energies of the three pharmaceuticals (in their most common speciation states) to model carbon surfaces with and without pyridinic/graphitic N dopants, as well as to perform classical or ab initio molecular dynamics simulations of adsorption at the water–carbon interface and, ideally, in situ spectroscopic confirmation (e.g., in situ FTIR or near-edge X-ray absorption fine structure spectroscopy).

ISSN No. 2454-6194 | DOI: 10.51584/IJRIAS |Volume XI Issue X October 2026

As such, Table 3 does not state any mechanism hierarchy; the mechanisms are presented in non-ranked, concurrent contributions whose relative weights cannot be determined from the current indirect measurements. The DFT and MD studies above will not be definitive until they are completed.

Competitive adsorption

For the equimolar ternary system (100 mg L^{-1} each; 0.5 g L^{-1} WBC-NK; solute-specific pH), the manuscript reports a measured uptake of TC of 152.3 mg g^{-1}, which is 19.7% lower than the condition-matched single-solute reference (189.7 mg g^{-1}, at the same C0, dose and pH; Table 2). The same was true when tested under a competitive condition of TC. The relative order of the uptake of the three compounds in the ternary mixture cannot be verified from the information provided here, as the UV–vis wavelength is common to all three compounds.

Model-based multi-solute (competitive) analysis.

Experimental isotherms were not measured for multi-solute, hence the constants of the extended-Langmuir model were estimated by assuming competitive adsorption ($q_i = q_{max,i} K_{L,i} C_{e,i} / (1 + \Sigma_j K_{L,j} C_{e,j})$) using the constants of single-solute isotherms of Table 2 for the equimolar ternary mixture of WBC-NK. The single solute references at each concentration were calculated using the same mass balance. The predicted competitive isotherm is summarized in table 5, and is made based on the extended-Langmuir assumptions (all solutes have the same site energetics, no solute–solute interactions in the adsorbed phase); the ideal adsorbed solution theory (IAST) fit to complete single-solute isotherms is recommended for experimental validation during the next phase.

Table 5. Extended-Langmuir predictions of competitive (equimolar ternary TC/CIP/DCF) adsorption on WBC-NK, computed from the single-solute Langmuir parameters of Table 2 with the batch mass balance at a dose of 0.5 g L^{-1}. All values are model predictions.

C_0 each (mg L^{-1})	q_{single} TC / CIP / DCF (mg g^{-1})	$q_{ternary}$ TC / CIP / DCF (mg g^{-1})	Decline TC / CIP / DCF (%)
25	48.9 / 48.3 / 48.0	48.6 / 47.8 / 47.4	0.8 / 1.1 / 1.2
50	97.7 / 96.2 / 95.2	94.7 / 92.2 / 90.7	3.0 / 4.2 / 4.8
100	194.3 / 189.4 / 185.5	150.8 / 133.5 / 124.7	22.4 / 29.5 / 32.7
150	288.8 / 275.1 / 261.3	168.8 / 137.2 / 123.1	41.6 / 50.1 / 52.9
200	379.0 / 340.8 / 305.7	177.8 / 137.6 / 120.8	53.1 / 59.6 / 60.5
400	561.3 / 399.9 / 337.6	191.6 / 137.0 / 116.5	65.9 / 65.8 / 65.5

The extended-Langmuir model is used to predict the uptake of TC at the tested ternary condition (100 mg L^{-1} each) of 150.8 mg g^{-1} which is close to the reported measured value of 152.3 mg g^{-1} (ca. 1.0 % difference). These are the predicted capacity losses from 22–33% at this loading (not actual CIP or DCF loss). Only a consistency check between the predicted and reported TC at one condition is an agreement sufficient to validate the model and to prove a specific competition mechanism. Predicted capacity loss is less than about 5% at lower modeled loadings (25–50 mg L^{-1} per solute) and these are well above typical environmental concentrations, and modelling at µg L^{-1} was not directly tested. Dissolved organic matter and other co-solutes also may be reflected in matrix effects in real effluent (Section 3.6).

There are no experimentally measured ternary CIP or DCF uptakes reported, whereas measured TC has been reported to decrease by 19.7% which does not represent the modeled CIP and DCF behavior. The extended-Langmuir analysis offers a preliminary predictive model, and is not an alternative to selective measurement.

The two major drawbacks of the principal multi-solute limitations are that only one ternary condition has been reported experimentally, and the multi-solute isotherm is model-predicted from single-solute parameters. Selective quantification and experimentally determined binary and ternary isotherms, including testing at environmentally realistic (μg L^{-1}) concentrations in real wastewater matrices, are required for validation.

Environmental stability

Regeneration. 88.3% (TC), 90.6% (CIP) and 92.1% (DCF) of the starting WBC-NK capacity was recovered after five cycles, with capacity loss confined to the first cycle (5–7%), possibly due to irreversible binding in ultra-micropores, and < 2% loss per cycle thereafter. Retentions comparable to KOH-modified sludge biochar (94.1% after 3 cycles) were observed, consistent with the good regenerability of alkaline-activated chars (Ding et al., 2024). No change in BET surface area (by < 3%) occurred over the five cycles.

Leaching. The total dissolved N-species concentration in the leachates of all materials were below 0.8 mg L^{-1} after 48 h at pH 7, and below 2.5 mg L^{-1} at pH 3 and 11. The low ash content of the wood feedstock is expected to limit the release of minerals, in comparison to sludge- or ash-derived chars (Ding et al., 2026). In this study, ash content was not analysed using proximate analysis, and the analysis of the leachate was done for dissolved N, K and P and not for a full trace metal screening (e.g., Fe, Zn, Cu, Pb, Cd). The low ash statement is therefore dependent on the composition of the wood feedstock, and quantitative ash and trace mineral leaching data identified as needed follow-up.

Aging. WBC-NK's fresh capacity for the three solutes was preserved at 84-89% after 30 days of wet–dry/oxidative aging, similar to the observations for oxidative aging of carbonaceous adsorbents (Alsawy et al., 2022), showing that both slight increases of surface oxygen (O content +2.6 at.%) and minor decreases of the pHpzc (6.9 → 6.3) occurred.

Real wastewater. In the spiked secondary effluent (DOC 11.2 mg L^{-1}), WBC-NK retained 81.5% (TC), 78.2% (CIP) and 80.4% (DCF) of its single-solute capacity, measured in the condition-matched ultrapure-water control experiments defined in Section 2.5 (5 mg L^{-1}, 0.5 g L^{-1}, pH 7.3, identical contact time), likely reflecting competition from dissolved organic matter and co-solutes. This 78–82% real matrix retention is higher than the ≥ 44.1% real water fraction reported by Xie et al. (2023) for H3PO4 functionalized biochar with diclofenac, but the two studies used different wastewater matrices, initial concentration and dose of adsorbent; hence, the results should not be compared directly to assess their performance.

Comparison with other biochars and activated carbon

Table 4. Reported capacities for pharmaceutical adsorption on functionalized biochars and activated carbon.

Adsorbent	**Pharmaceutical**	**q_{max} (mg g^{-1})**	**Reference**
N-doped KOH-activated wood biochar (this work)	Tetracycline	588.6	This study
KOH-activated walnut-shell biochar	Tetracycline	607.0	Shi et al. (2023)
P-doped KOH-activated microalgal biochar	Tetracycline hydrochloride	662.9	Liu et al. (2025)
KOH-activated reed biochar	Tetracycline	> 20× pristine (fold increase; no absolute q_{max} reported)	Zhao et al. (2020)
MnAl-LDH/KOH biochar composite	Tetracycline	1477.7	Fan et al. (2024)

H_3PO_4-functionalized fish-scale biochar	Diclofenac sodium	967.1	Xie et al. (2023)
Engineered wood sponge	Tetracycline / DCF	863.8 / 321.3	Godiya & Leiviskä (2025)
Wood-derived biochar (review range)	Sulfamethoxazole	≤ 397.2	Godiya & Leiviskä (2025)
Biochar class (meta-range)	Ibuprofen	2.5–1033	Osman et al. (2024)
Activated carbon (meta-range)	Ibuprofen	10.8–408	Osman et al. (2024)

The literature values in Table 4 are provided from various feedstocks, activation procedures, experimental conditions and isotherm models, and thus cannot be considered as a controlled standard, and should not be interpreted as a declaration of superiority of the adsorbent in question over any other adsorbent. The value of WBC-NK capacities is within the range of the most reported KOH/N-doped chars, but also provides potential feedstock-utilization benefits, but a carbon advantage was not quantified in this study (Godiya & Leiviskä, 2025). Matched performance, regeneration and end-of-life accounting (Pal et al., 2026) would be the subject of a full techno-economic comparison, but this was not undertaken in this study.

Indicative reagent economics and sustainability considerations

The functionalization pathways were evaluated in an indicative way by considering bulk chemical prices, namely KOH (approx. USD 0.8-1.2 kg^{-1}), urea (approx. USD 0.3- 0.5 kg^{-1}) and H3PO4 (85%) (approx. USD 0.9-1.3 kg^{-1}). Due to the impregnation ratio of 1:3 (mass of biochar:mass of KOH), the chemical cost is estimated to be USD 2.4–3.6 kg^{-1} before taking into account the washing loss and 18.9% activation yield, which is USD 13–19 kg^{-1} on a finished-adsorbent basis. The extra urea needed is a 1:2 biochar:urea ratio, or approximately USD 0.6-1.0kg^{-1} biochar, and the total cost per kg pristine char is USD 3.0-4.6 (estimated cost after dividing by the yield of 16.8%). The numbers in this analysis are estimates, as they do not include energy, capital, labor, wash water treatment and spent chemicals management costs, which generally contribute to most of the overall production costs; a complete techno-economic and life-cycle assessment is not part of this study. The use of chemical recovery from the alkaline wash liquors, such as K2CO3/KOH recycling, is often suggested in the activated-carbon industry and would make a significant reduction in these figures, but was not used here. The estimates are made using reagents only and not from the cited market prices for commercial activated carbon and hence do not provide any indication as to cost competitiveness; feasibility of the co-activation route at the process level (energy demand of the 800 °C activation step, wash-water volumes) must be demonstrated prior to any scale-up claim.

The two-step thermal route also has a significant environmental impact. Here, the total of reaction enthalpy, furnace losses and the 800 °C activation step is not quantified and not measured, only the sensible heat input of 0.9 MJ kg^{-1} for the feedstock to sensible heating alone is required. The additional energy demand of the next step, namely the activation under KOH/N-doping at 800 °C, would also be proportional to the KOH loading, which is 1:3. In N2 pyrolysis, a permanent gas fraction is generated, containing H2, CH4, CO and CO2, and a condensable bio-oil, both of which could be used as fuel to offset process heat in a designed process; off-gassing from KOH activation would result in CO and K vapour (which could be oxidized to K2CO3). These streams were vented at laboratory scale and there is no direct emission inventory reported here. On the credit side, the process is able to retain a significant part of the feedstock carbon in a stable char (27.4% of the dry feedstock mass as WBC), and Pine Sawdust is a waste product of low value, allowing for no competition with land use. Future work is identified as a comparative life-cycle assessment with commercial activated carbon, which includes the fate of the adsorbed pharmaceuticals and the disposal/regen of spent-adsorbent. In this work no quantitative carbon-advantage claims is made, and a full energy and emissions inventory is identified as a required future work.

Two additional sustainability trade-off for the synthesis route are recognized. First, the successive washing with 0.1 M HCl produced chloride containing wash-water containing fine carbon particles and K, which, at industrial scale, would have to be neutralised and treated, and such wash-water recycling was not conducted at laboratory scale. Second, the off-gases were vented, and only the N remaining in the char (4.1 at.%, Table 1) was measured, so a mass balance of N (urea-N fed vs. N retained in char vs. N off-gas) was not performed and is recognized as a gap. The energy-intensive use of urea as a synthetic fertilizer is a footprint that should be compared to the ~1.25–1.3-fold capacity increase that it brings (i.e. WBC-K to urea) and lower dose of doping should be explored.

Study limitations

Avoiding pitfalls of the multi-solute limitation mentioned in Section 3.5: only one ternary condition is reported experimentally and the multi-solute isotherm is predicted from single solute parameters.

CONCLUSIONS

The adsorption of tetracycline, ciprofloxacin and diclofenac sodium using pristine pine-sawdust biochar, KOH-activated biochar, H3PO4-activated biochar and N-doped KOH-activated biochar were compared in this laboratory scale study. WBC-NK had the highest BET surface area (512.9 m^2g^{-1}) and the highest fitted Langmuir maximum adsorption capacities of 588.6, 412.3 and 346.8 mg g^{-1} of TC, CIP and DCF, respectively, which are model derived values based on the measured concentration range and should be interpreted with the assumptions of the Langmuir model.

The dual characterization and adsorption results suggest that the contributions of surface chemistry, pore structure and solution conditions are present, including π–π EDA interactions, hydrogen bonding, electrostatic interactions, hydrophobic interactions, and pore filling, which are possible. These are not confirmed molecular-scale interpretations, but rather. Modeling was performed with single-solute isotherms in the extended-Langmuir analysis, and the predictions were found to be competitive, below about 5% at lower loadings (25–50 mg L^{-1} per solute) which are not representative of typical environmental concentrations (µg L^{-1}). The model prediction at 100 mg L^{-1} per solute was close to the reported ternary TC uptake, but one-point agreement is not a way to validate the model. The need for selective analytical confirmation and measured multi-solute isotherms, particularly for CIP and DCF, is essential.

Regeneration (88.3–92.1% capacity retention – demonstrated over 5 cycles) and leaching (less than 0.8 mg L^{-1} at pH 7) results, as well as aging and secondary-effluent tests (at least 78% capacity retention relative to condition-matched single-solute tests) suggest good stability and matrix robustness at a bench scale, subject to verification against the original test results. The major drawbacks are the use of one reported ternary competition condition, the use of model-derived multi-solute isotherms instead of measured, the lack of selective quantification of CIP and DCF in mixtures, the lack of a full techno-economic/life-cycle assessment, and indirect mechanistic evidence. Future work should include experimental multi-solute and competitive isotherm experiments under environmentally relevant concentrations to validate the extended-Langmuir predictions, DFT and MD mechanistic studies, continuous-flow experiments to validate, end-of-life management of spent-adsorbent and strategies for waste management (wash-water and off-gas), a full techno-economic (TE) and life-cycle analysis (LCA) against commercial activated carbon, and end-of-life management of spent-adsorbent and strategies for waste management (wash-water and off-gas). The present laboratory results are not intended to imply industrial scale applicability.

Declarations

Conflict of interest: The author declares no conflict of interest.

Funding: This research received no external funding.

Data availability: Data supporting the findings are available from the corresponding author upon reasonable request.

REFERENCES

1. Alsawy, T., Rashad, E., El-Qelish, M., & Mohammed, R. H. (2022). A comprehensive review on the chemical regeneration of biochar adsorbent for sustainable wastewater treatment. *npj Clean Water, 5*, Article 29. https://doi.org/10.1038/s41545-022-00172-3
2. Chauhan, S., Shafi, T., Dubey, B. K., & Chowdhury, S. (2023). Biochar-mediated removal of pharmaceutical compounds from aqueous matrices via adsorption. *Waste Disposal & Sustainable Energy, 5*, 37–62. https://doi.org/10.1007/s42768-022-00118-y
3. Ding, J., Liang, J., Wang, Q., Tan, X., Xie, W., Chen, C., Li, C., Li, D., Li, J., & Chen, X. (2024). Enhanced tetracycline adsorption using KOH-modified biochar derived from waste activated sludge in aqueous solutions. Toxics, 12(10), Article 691. https://doi.org/10.3390/toxics12100691
4. Ding, P., Lu, J., Xu, L., Zhou, Q., Jiang, M., Yan, Z., & Yang, P. (2026). Recent advances in modified biochars for the adsorptive removal of typical antibiotics from water: A comparative review of performance, influencing factors, and underlying mechanisms. *RSC Advances*. https://doi.org/10.1039/D6RA06945B
5. Fan, X., Wang, S., Zhang, W., Fan, X., Huang, Z., Zhou, N., & Xu, H. (2024). KOH-activated biochar loaded with MnAl-layered double hydroxides for superior adsorption of tetracycline from the aquatic environment. *Journal of Industrial and Engineering Chemistry, 134*, 474–483. https://doi.org/10.1016/j.jiec.2024.01.010
6. Godiya, C. B., & Leiviskä, T. (2025). Wood-derived adsorbents for the removal of pharmaceutical contamination from wastewater: A review. *Environmental Chemistry Letters*. https://doi.org/10.1007/s10311-025-01886-9
7. Laishram, D., Kim, S.-B., Lee, S.-Y., & Park, S.-J. (2025). Advancements in biochar as a sustainable adsorbent for water pollution mitigation. *Advanced Science, 12*(19), Article e2410383. https://doi.org/10.1002/advs.202410383
8. Liu, B., Li, W., Huang, Y., Qin, W., Wang, M., Jia, Y., Xu, H., Qu, L., Jiang, H., Wang, C., & Ma, Z. (2025). Enhanced tetracycline hydrochloride removal by ultra-microporous phosphorus-doped KOH-activated microalgal biochar: Adsorption performance and mechanistic insights. *Environmental Research, 287*, Article 123040. https://doi.org/10.1016/j.envres.2025.123040
9. Nand, S., Singh, P. P., Verma, S., Mishra, S., Patel, A., Shukla, S., & Srivastava, P. K. (2025). Biochar for mitigating pharmaceutical pollution in wastewater: A sustainable solution. *Science of the Total Environment, 966*, Article 178743. https://doi.org/10.1016/j.scitotenv.2025.178743
10. Nguyen, V. D., Luu, T. A., Chang-Chien, G., & Le, V. G. (2025). Progress in biochar-derived adsorbents: Preparation, modification strategies, and applications in remediation of antibiotics from wastewater. *Materials Advances, 6*, 8839–8876. https://doi.org/10.1039/D5MA00872G
11. Osman, A. I., Ayati, A., Farghali, M., Krivoshapkin, P., Tanhaei, B., Karimi-Maleh, H., Krivoshapkina, E., Taheri, P., Tracey, C., Al-Fatesh, A., Ihara, I., Rooney, D. W., & Sillanpää, M. (2024). Advanced adsorbents for ibuprofen removal from aquatic environments: A review. *Environmental Chemistry Letters, 22*(1), 373–418. https://doi.org/10.1007/s10311-023-01647-6
12. Pal, A., Das, S., Paul, S. R., et al. (2026). Cost analysis and adsorption efficiency of chemically activated biochar from rubber wood sawdust for ciprofloxacin removal in environmental remediation. *Biomass Conversion and Biorefinery, 16*, Article 84. https://doi.org/10.1007/s13399-025-07048-9
13. Qiang, Z., & Adams, C. (2004). Potentiometric determination of acid dissociation constants (pKa) for human and veterinary antibiotics. *Water Research, 38*(12), 2874–2890. https://doi.org/10.1016/j.watres.2004.03.017
14. Sajjadi, B., Zubatiuk, T., Leszczynska, D., Leszczynski, J., & Chen, W. Y. (2019). Chemical activation of biochar for energy and environmental applications: A comprehensive review. *Reviews in Chemical Engineering*. https://doi.org/10.1515/revce-2018-0019
15. Shi, Q., Wang, W., Zhang, H., Bai, H., Liu, K., Zhang, J., Li, Z., & Zhu, W. (2023). Porous biochar derived from walnut shell as an efficient adsorbent for tetracycline removal. *Bioresource Technology, 383*, Article 129213. https://doi.org/10.1016/j.biortech.2023.129213
16. Shirani, Z., Carrasco-Navarro, V., & Sorvari, J. (2025). Effective adsorption of pharmaceuticals by plant-based activated biochar. *Water, Air, & Soil Pollution, 236*, Article 872. https://doi.org/10.1007/s11270-025-08526-6

17. Simonin, J.-P. (2016). On the comparison of pseudo-first-order and pseudo-second-order rate laws in the modeling of adsorption kinetics. *Chemical Engineering Journal, 300*, 254–263. https://doi.org/10.1016/j.cej.2016.04.079
18. Tangestani, E., Kumar, R., Miller, C. M., & Antunes, E. (2026). Recent advances on application of modified biochar for the removal of pharmaceutical compounds from wastewater. *ChemistryOpen, 15*(6), Article e70221. https://doi.org/10.1002/open.20270221
19. Xie, J., Liu, M., He, M., Liu, Y., Li, J., Yu, F., Lv, Y., Lin, C., & Ye, X. (2023). Ultra-efficient adsorption of diclofenac sodium on fish-scale biochar functionalized with H_3PO_4 via synergistic mechanisms. *Environmental Pollution, 322*, Article 121226. https://doi.org/10.1016/j.envpol.2023.121226
20. Zhao, C., Ma, J., Li, Z., Xia, H., Liu, H., & Yang, Y. (2020). Highly enhanced adsorption performance of tetracycline antibiotics on KOH-activated biochar derived from reed plants. *RSC Advances, 10*, 5066–5076. https://doi.org/10.1039/C9RA09208K